Upstream Influence and Separation Scales in Fin-Induced Shock Turbulent Boundary-Layer Interaction

D. S. Dolling* and P. E. Rodi†
University of Texas at Austin, Austin, Texas

An experimental study has been made of the effects of leading-edge geometry on the upstream influence and separated flow length scales in fin-induced shock wave turbulent boundary-layer interaction. The fins used had wedge-shaped, hemicylindrical and elliptic leading edges and were tested under adiabatic conditions at Mach 4.9. The primary objective was to determine if the length scales generated by different leading edges could be understood within a common framework. To a first approximation the normalized centerline length scales correlate with fin leading-edge drag coefficient. Attempts to correlate additional data at Mach 1.98 and 2.48 from other studies resulted in a reasonable correlation for upstream influence, but that for the separation length showed a clear influence of Mach number. The fact that the upstream influence can be reasonably well correlated in this form lends further support to the view that large-scale three-dimensional vortical separated flows of this type may be largely inviscid dominated.

Nomenclature

b = half major axis of elliptical leading edge
C_D = drag coefficient
C_f = skin friction coefficient
C_p = pressure coefficient $(P-P_\infty)/q_\infty$
D = hemicylindrically blunted fin leading-edge diameter
L_u = upstream influence on fin centerline
L_{sep} = distance from fin leading edge to primary separation line, on centerline
M = Mach number
P = pressure
q = dynamic pressure
Re = Reynolds number
t = fin thickness
u = streamwise velocity
u^+ = u/u_τ
u_τ = friction velocity $(\sqrt{\tau w/\rho})$
X,Y,Z = streamwise, spanwise, and vertical coordinate measured from fin leading edge (Fig. 2)
X_{sep} = streamwise distance between primary separation line and trace of inviscid bow shock (Fig. 2)
y^+ = $\frac{u_\tau \gamma}{v}$
γ = ratio of specific heats
δ = boundary-layer velocity thickness
δ^* = boundary-layer displacement thickness
Δ = shock detachment distance
θ = boundary-layer momentum deficit thickness
θ_d = shock detachment angle
θ_L = half-angle of wedge-shaped leading edges
v = kinematic viscosity
Π = wake strength parameter
ρ = density
τ = shear stress

Subscripts

CL = centerline
max = maximum value
o = value in undisturbed boundary layer
w = at the wall
∞ = freestream conditions

Received June 15, 1986; revision received Aug. 24, 1987. Copyright © American Institute of Aeronautics and Astronautics, Inc., 1987. All rights reserved.

*Associate Professor, Department of Aerospace Engineering and Engineering Mechanics. Associate Fellow AIAA.
†Graduate Student, Department of Aerospace Engineering and Engineering Mechanics. Student Member AIAA.

Introduction

In shock wave turbulent boundary-layer interactions induced by semi-infinite circular cylinders or hemicylindrically blunted fins, a large-scale, three-dimensional vortical flowfield is generated. Figure 1 illustrates the complexity. On the centerline, fluid particles separate, roll up into a vortex (Fig. 1b) and spiral outboard in a horseshoe vortex system resulting in the classic limiting streamline pattern shown in Fig. 1c. In such flows it is well known that many of the important flow length scales depend primarily on the cylinder or fin leading-edge diameter D.[1-5] One such scale is the centerline upstream influence L_u, which is typically in the range 2 to $3D$. Another is the centerline separated flow length scale L_{sep}, defined as the distance from the leading edge to the primary separation line. The spanwise development of the flowfield, as well as its vertical extent, also depends primarily on D.[6] Freestream Mach number M_∞ and incoming boundary-layer properties ($Re_{\delta o}$ and C_f) have only a secondary effect on the scaling. However, the state of the boundary layer is critical. For laminar flows L_u and L_{sep} both increase by a factor of 3 to 4, although the appropriate scaling parameter is still D.[7,8] These observations are supported by data from a large number of experimental studies at speeds from transonic to hypersonic, as well as by numerical simulations.[9,10]

The use of D as a correlation parameter is convenient and provides a means of making quick estimates of interaction length scales. However, its use masks the underlying physics of the interaction. A simple example demonstrates this. Under identical flow conditions, a fin of thickness t with a flat leading edge generates a similar flow structure (as inferred from wall pressures and surface streak patterns), but one in which L_u and L_{sep} are about twice those for a hemicylindrical fin with $D=t$.[11] Any attempt to explain these two results within a common framework immediately raises the question of which parameters control the interaction length scale. It is not local shock strength, because on the centerline the shocks for both leading edges are detached and at the same M_∞ both have the same strength. Moreover, this independence of shock strength is evident from earlier studies (e.g., Ref. 1) using hemicylindrical fins in which it was shown that large changes in M_∞ had only a secondary effect on the scale. Similar to the

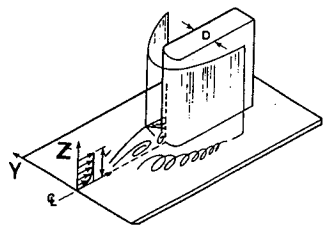

Fig. 1a Blunt fin-induced flowfield.

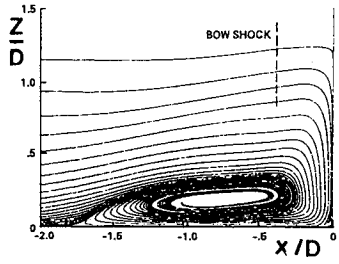

Fig. 1b Computed particle paths on centerline.

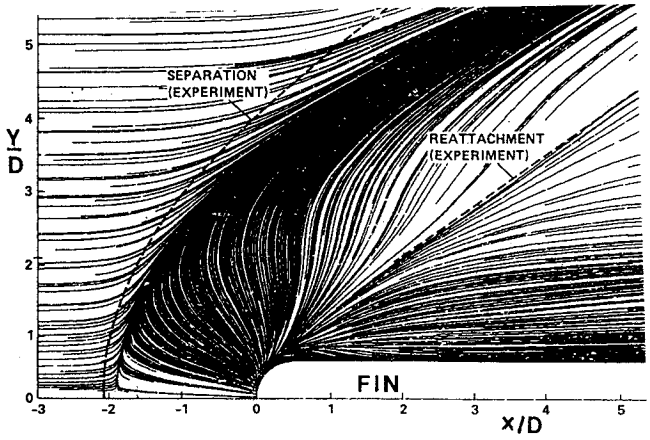

Fig. 1c Computed surface streak pattern (from Ref. 10).

hemicylindrical fin case (see Refs. 11 and 12), as well as the current work, show that L_u for a flat fin can also be correlated in terms of a geometric parameter, namely t. Again, this is a simple and convenient result, but provides no physical explanation of why the interaction scale doubles, nor does it further our ability to predict the scales for an arbitrary leading-edge shape.

This same question arises in attempting to explain or correlate the measurements of Saida who tested several fins with wedge-shaped leading edges at $M_\infty = 1.98$ and 2.48.[12] Depending on the wedge angle, interactions with a wide range of scales were generated (including one which was the same as that for a hemicylindrical leading edge). Saida found that L_u and L_{sep} increased linearly with the wedge half-angle θ_L with a separate curve for each Mach number. In summary, it appears that the data for different leading-edge shapes can be correlated, but only in terms of the particular geometric parameter that describes them (i.e., D, t, or θ_L). The fundamental question of whether these measurements (and others for different leading-edge shapes) can be understood within some common framework in which the length scales are not related to the leading-edge geometry but to the inviscid shock properties has not, as far as is known, been addressed. This is the subject of the experimental study described in this paper.

In this test program, centerline wall-pressure distributions, primary separation location, and upstream influence have been measured in interactions at Mach 5 generated by

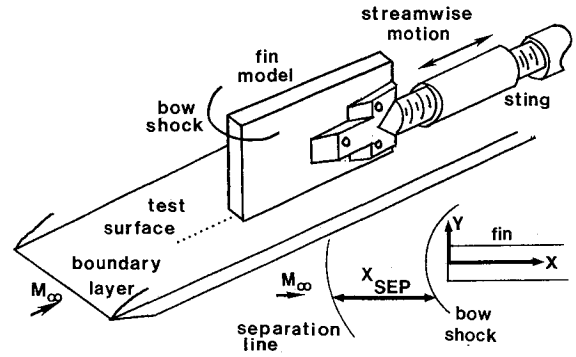

Fig. 2 Model and coordinate system.

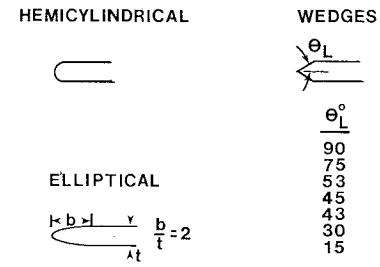

Fig. 3 Fin leading-edge geometries.

semi-infinite blunt fins of constant thickness but with different geometry leading edges. The primary objective of the study was to address the question raised previously. The secondary objectives were to determine 1) the effects of attached and detached shocks on the surface pressure distribution and the inferred flow structure, and 2) the effects of shock properties on the spanwise growth rate of the separated flow.

Experimental Techniques

Wind Tunnel and Models

The tests were made in the 7 in. × 6 in. (18 cm × 15 cm) variable stagnation temperature blowdown tunnel at the University of Texas' Balcones Research Center. The model and the coordinate system used for data presentation are shown in Fig. 2. The test surface was a full-span horizontal flat plate with a sharp leading edge. It was instrumented with a single streamwise row of pressure taps 0.012 in. (0.03 cm) in diameter which were spaced at 0.20 in. (0.51 cm) intervals.

Nine different fins were tested, and the leading-edge geometries are shown in Fig. 3. Wedge angles given by $\theta_L = 15$ and 30 deg were selected to provide relatively weak attached shock waves (the detachment angle, $\theta_d = 40.9$ deg at $M_\infty = 4.9$). $\theta_L = 45$ deg was selected as a value just above θ_d. $\theta_L = 75$ and 90 deg were chosen to provide strong detached shock waves. The 43- and 53-deg models were built after the initial tests were made because the results indicated that these angles would generate interactions with approximately the same upstream influence as the elliptic and hemicylindrical leading edges, respectively. Hence, the spanwise development of flows with the same centerline length scale (but generated by different leading edges) could be examined.

All of the fins were nominally 0.25 in. thick (0.64 cm), 4 in. long (10 cm), and 3.0 in high (7.7 cm). Based on the criterion of Ref. 4, their height was effectively semi-infinite. The fins were held in position using a small screwjack between the upper surface of the fin and the test section ceiling. For all tests, the fin leading edge was located between 10.5 in. (26.7 cm) and 10.7 in. (27.2 cm) downstream of the test surface leading edge.

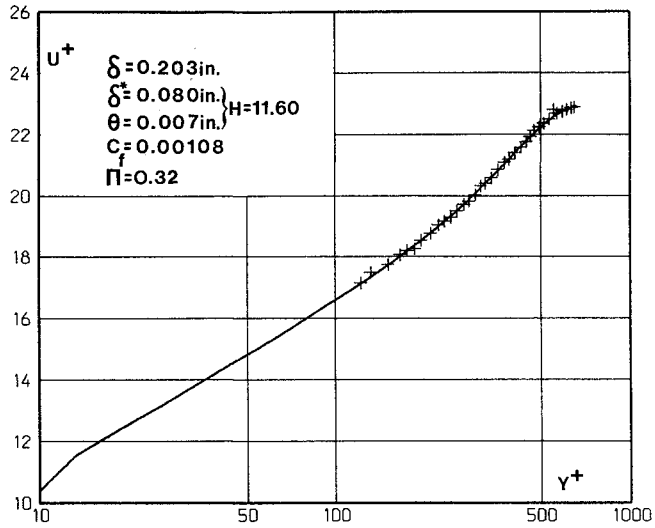

Fig. 4 Incoming turbulent boundary-layer mean velocity profile and properties.

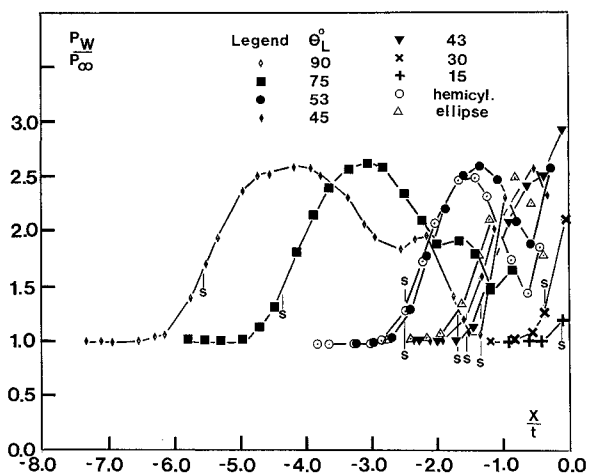

Fig. 5 Centerline wall pressure distributions.

Test Conditions and Incoming Boundary Layer

At the test station, the nominal freestream Mach number is 4.9. The stagnation pressure for all tests was 300 psia (2.07×10^6 Nm^{-2}) $\pm$ 1% and the stagnation temperature was 338 K $\pm$ 1%, giving a nominal freestream Reynolds number of 52×10^6 m^{-1}(16×10^6 ft^{-1}). The wall temperature was within 5% of the adiabatic value for all tests.

Since the fin leading edge was approximately 11 in. (26 cm) downstream of the test surface leading edge, a trip was used to ensure that the incoming boundary layer was fully turbulent. The trip was full span and consisted of a 0.5 in. (1.27 cm) wide strip of 80 grit emery cloth located approximately 0.5 in. (1.27 cm) downstream of the plate leading edge. Pitot surveys were made at several stations to examine the state of the incoming boundary layer. The incoming mean velocity profile plotted in wall coordinates u^+ vs y^+ matches well the combined wall-wake law (Fig. 4). The skin-friction coefficient is within 5% of the value predicted by the Van Driest II theory.

Measurements

Only a brief description of the measurement techniques is given here. Full details are provided in Ref. 13. Wall pressures were measured using a PDCR23D pressure transducer referenced to a vacuum installed in a scanivalve. To improve the spatial resolution of pressure distributions, several runs were made with the fin leading edge at different streamwise stations. Over the range of travel ($\approx$0.2 in.), the change in incoming flow conditions had a negligible effect on the interaction. All tests were made at zero angle of attack.

The location of the primary separation line was obtained using the kerosene-lampblack surface tracer technique.[13] Details of the method are given in Ref. 14. It has two advantages over the conventional oil-streak technique. First, the separation line is very clearly defined. No smearing occurs because the tunnel is not shut down until the kerosene has evaporated. Second, the patterns are lifted off the surface on sheets of transparent tape, so that full-scale, undistorted records are obtained. The repeatability was excellent.

Since the inviscid shock wave position is used as a reference, it was critical that the shock shapes be known accurately. With the flat plate removed from the tunnel, the fins were rotated to a horizontal position and the shock shapes obtained from shadow photographs.

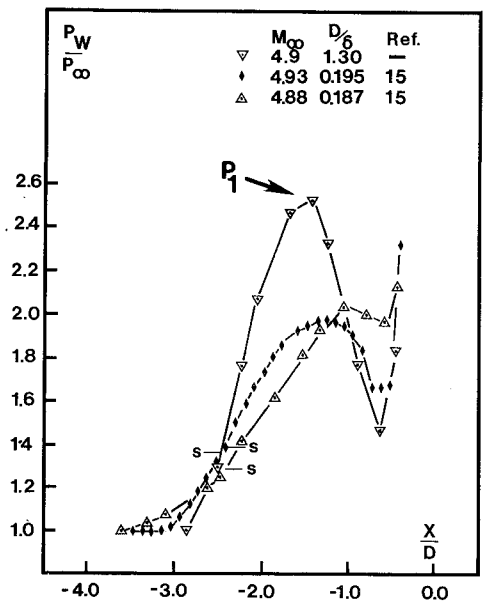

Fig. 6 Comparison of current hemicylindrical data with those of Ref. 15.

Discussion of Results

Pressure Distributions

Normalized centerline pressure distributions for the nine leading edges are shown in Fig. 5. In each case, the separation location is indicated by an S. The data for the hemicylindrical leading edge can be compared directly with results from other studies. The normalized upstream influence, L_u/D, agrees well with the correlation of Ref. 4 which is based on data from 12 studies at Mach numbers from 2 to 5. Figure 6 shows the current pressure measurements and those of Winkelmann,[15] also at Mach 5. The trends of decreasing L_u/D and increasing peak pressure P_1 (defined in Fig. 6) with increasing D/δ are both consistent with earlier work at Mach 3 in which the effects of this ratio were investigated systematically.[11]

The peak level P_1 reflects the pressure rise through the separation shock wave and increases with D/δ, because of the dominance of D in controlling L_u (typically, $L_u/D \approx 2$–3.5, independent of δ). For small D/δ, the entire separation shock wave is either partially or fully immersed in the lower (on average) Mach number fluid in the incoming boundary layer. It can be argued that for such a case the pressure rise will be less than if a large fraction of the shock was in the higher Mach number fluid of the external flow as is the case for large

D/δ. For large D/δ, the inference is that P_1 will reach a constant level. Experiments confirm this and show that it occurs for $D/\delta \approx 4$–5. The fact that P_1 is constant for the current tests (at least for $\theta_L > 43$ deg) is consistent with the above discussion. With t/δ fixed (≈ 1 in this case), L_u/t is ≥ 2 such that the major fraction of the separation shock forms in the constant Mach number fluid outside of the boundary layer and has the same overall strength in all cases.

For $\theta_L = 15$ and 30 deg, the upstream influence is small, and the details of the pressure distributions are not well resolved. However, comparison with Saida's experiments in which the spatial resolution for small θ_L was superior, supports the assumption that the pressure rises continuously from the interaction start X_o to the fin root. At $\theta_L = 43$ deg (2 deg above θ_d), a well-defined kink appears in the distribution at $X/t \approx -0.5$. By $\theta_L = 45$ deg, the classical "peak-trough" shape associated with the horseshoe vortex system has evolved. Thus, it appears that this shape, which is characteristic of interactions generated by hemicylindrically blunted fins and circular cylinders, does not develop until θ_L is close to, or equal to θ_d. With a further increase in θ_L, the scale increases, but there is no apparent change in flow structure until $\theta_L = 75$ deg when a secondary peak, indicative of a secondary vortex, develops. Preliminary numerical computations also show this vortex.[16] As θ_L increases to 90 deg, the scale increases further, but the distributions are essentially geometrically similar, implying that, in this range, changes in θ_L only produce a stretching effect.

In Fig. 7, the X origin has been shifted from the fin root to the interaction start. For clarity, not all of the distributions are shown. It can be seen that the length scale of the pressure rise through separation is the same, as are the pressure levels. Recent work using hot films[17] and fast response Kulite pressure transducers[18] in similar interactions generated by circular cylinders shows that the separation shock is unsteady and undergoes a large-scale motion of $O[D]$ in the streamwise direction. As a consequence, the wall pressure signal is intermittent from X_o to close to S. It is the large amplitude shock-induced pressure fluctuations superimposed on the undisturbed boundary-layer pressure signature which generates the mean wall pressure rise through separation. The implication of Fig. 7, and the earlier observation of the constancy of the level P_1, is that the same unsteady shock system occurs in all the cases studied, and it is progressively shifted upstream with increasing θ_L.

The question of what drives the shock motion is not entirely resolved. From conditional sampling of the wall pressure signal in a Mach 3, separated compression ramp flow which exhibits a similar unsteadiness, Andreopoulos and Muck suggested that the shock motion was triggered by the bursting phenomenon in the incoming boundary layer.[19] This conclusion was based on the observation that the shock zero-crossing frequency was the same order as the estimated bursting frequency. More recent work in flows induced by circular cylinders in the authors' test facility and analysis of earlier hemicyclindrically blunted fin data from the Princeton University Mach 3 blowdown tunnel[18] do not support this observation. The zero-crossing frequency was found to be an order of magnitude less than the estimated bursting frequency. The low frequencies, coupled with a dependence on the properties of the downstream separated flow, suggest a connection with the latter, rather than with the turbulence of the incoming boundary layer.

Separated Flow and Upstream Influence Length Scales

L_{sep} and L_u normalized by t are shown vs θ_L in Figs. 8 and 9, respectively. The shock-detachment angle is indicated by θ_d. L_u was determined from the pressure distributions. For consistency, the upstream limit of disturbed flow was taken as being where the tangent to the initial pressure rise intersects the horizontal line representing the undisturbed pressure level.

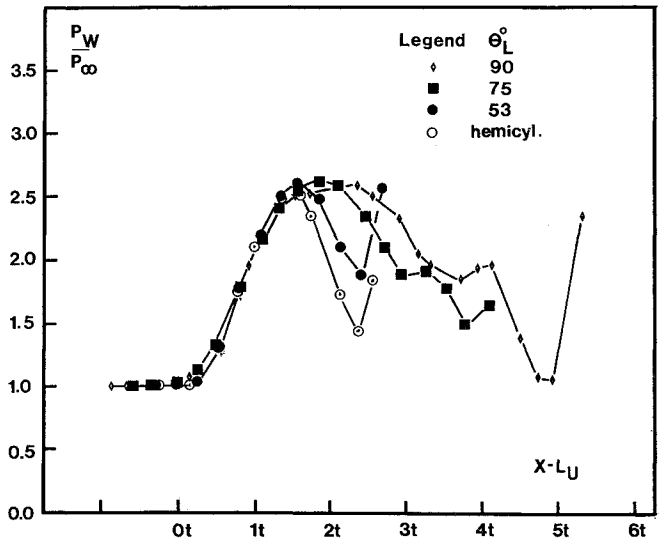

Fig. 7 Centerline wall pressure distributions with X axis origin displaced to interaction start.

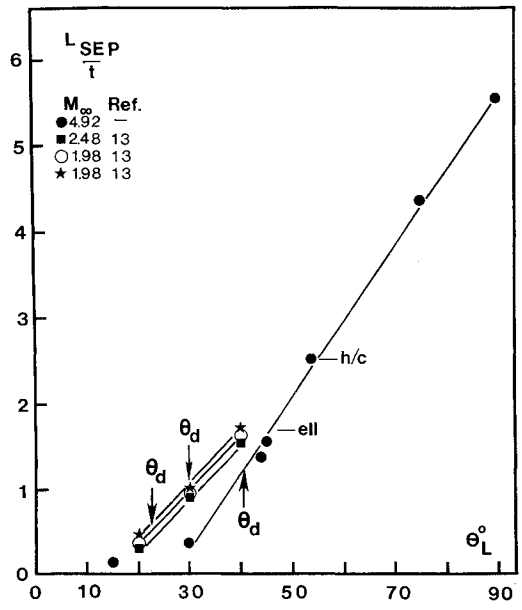

Fig. 8 Centerline separated flow length as a function of θ_L.

For $\theta_L \approx 30$ deg, L_{sep}/t and L_u/t increase linearly at approximately the same rate (≈ 0.09 per deg). In neither case is there a deviation from the linear trend as the inviscid shock detaches from the fin leading edge. Saida's data are also shown, as is the single data point obtained by Dolling and Bogdonoff.[11] at Mach 3 for $\theta_L = 90$ deg. Saida's results, as noted earlier, are also linear. As expected, the upper data set at $M_\infty = 1.98$ is for the smaller D/δ. For large θ_L and for fixed t/δ, the effect of Mach number on L_u is small. For $\theta_L = 90$ deg, L_u/t varies by less than $\pm 7\%$ about the mean value for Mach numbers of 2 and 5.

If the value of L_u/t generated by the hemicylindrical leading edge (indicated by "h/c") is now located on the straight line fit in Fig. 9, it corresponds to $\theta_L \approx 53$ deg. If L_{sep}/t for the hemicylindrical case is then plotted at $\theta_L \approx 53$ deg in Fig. 8, it agrees well with the wedge data. (Similarly, the elliptical leading edge, indicated by "ell" corresponds to $\theta_L = 45$–47 deg.) Hence, interactions generated by a hemicylindrical model and a 53 deg wedge model have the same

upstream influence and separated flow-length scales. This result correlates with the shock shape behavior for these two leading edges. First, as shown in Fig. 10, both shapes have the same shock detachment distance Δ. Second, close to the centerline the two shocks are almost spatially coincident. This can be seen in Fig. 11, which shows the trace of the inviscid shock wave on the test surface and also the corresponding primary separation line. The primary separation lines for $\theta_L = 53$ deg and the hemicylindrical fin are coincident out to $Y/t \approx 1.0$ (as are the shocks approximately), then diverge (as do the shocks). The separation line for the hemicylindrical case is the more highly swept, as is its shock wave.

Although the two separation lines diverge with increasing Y/t, the spanwise growth rates of the separated flow-length scale upstream of the shocks are the same. Figure 12 shows the difference between the centerline value of X_{sep} (defined as the streamwise distance from the primary separation line to the inviscid bow shock) and that at a given spanwise station as a function of Y/t. The growth rate is not only the same for $\theta_L = 53$ deg and the hemicylindrical case, but is essentially the same for all leading edges (approximately one fin thickness t for each spanwise increment of one fin thickness). Inspection of the shock shapes (Fig. 11) shows that this is not entirely surprising. For $Y/t > 1.5$–2.0, all of the shocks are highly swept, and are almost parallel; they are simply displaced upstream with increasing θ_L.

Because the spanwise growth rate of the separated flow is the same for all leading edges, then it is the centerline scale that sets up the length scales throughout the interaction. The preceding results show that spatially coincident shocks generate the same centerline length scales, which provide a first indication that the scales can be related to the inviscid shock properties. This is a partial answer to the question raised in the introduction, but is only qualitative and does not indicate the form of the relationship. Because the centerline scale does not depend on such local properties as the centerline pressure rise, but is the same when the shocks are coincident over a region near the centerline, this suggested that some average or integrated shock property evaluated over this region might have a controlling influence.

Several ideas were examined. First, the shock wave shapes were least-squares curve fitted. Attempts were made to correlate L_u and L_{sep} with the average shock wave angle between the centerline and some specified spanwise station. The latter included the intersection point of the sonic line and the bow shock, and the location of a specified shock wave angle. These approaches were not successful. The shock stand-off distance was also considered, but since it is very difficult to measure accurately, particularly for small θ_L, and also was not known for the lower Mach number data, it was not used. Further, the experimental data show no evidence of any abrupt changes in flow-length scales as the shock detaches, suggesting that the appropriate correlation parameter would be equally valid for both shock conditions. Second, correlation with the fin leading-edge drag coefficient C_D was attempted. For fins with attached shock waves, C_D was calculated from oblique shock-wave theory. For the detached shock cases at Mach 5, modified Newtonian theory was used with C_p given by

$$C_p = C_{p_{max}} \sin^2 \theta_b \tag{1}$$

where θ_b = the local body angle relative to the undisturbed flow direction, and $C_{p_{max}}$ is the pressure coefficient determined using the stagnation pressure downstream of the normal shock wave and is given by

$$C_{p_{max}} = \frac{2}{\gamma M_\infty^2}\left\{\left[\frac{(\gamma+1)^2(M_\infty)^2}{4\gamma M_\infty^2 - 2(\gamma-1)}\right]^{\gamma/\gamma-1}\left[\frac{1-\gamma+2\gamma M_\infty^2}{\gamma+1}\right]-1\right\} \tag{2}$$

Unlike unmodified Newtonian theory, in which $C_p = 2\sin^2\theta_b$, the use of $C_{p_{max}}$ introduces the effect of Mach number. Further, it is well known that for predicting pressures on blunt noses modified Newtonian theory is more accurate than unmodified Newtonian and works quite well even at relatively low Mach numbers. For the detached shock cases at $M_\infty = 1.98$ and 2.48, C_D was calculated using the semiempirical correlation technique of Ref. 20. The drag coefficient is given by

$$C_D = KC_p' - 2(1-K)/\gamma M_\infty^2 \tag{3}$$

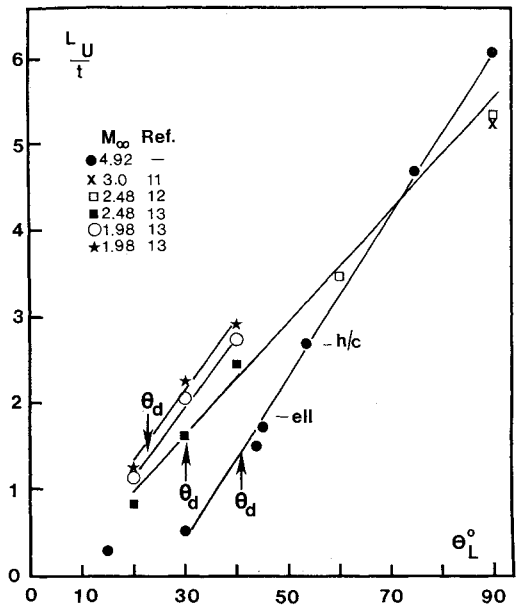

Fig. 9 Centerline upstream influence as a function of θ_L.

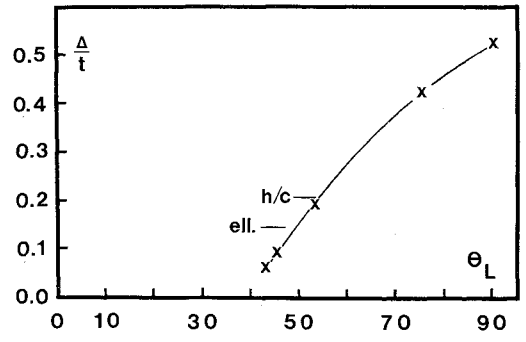

Fig. 10 Shock detachment distance as a function of θ_L.

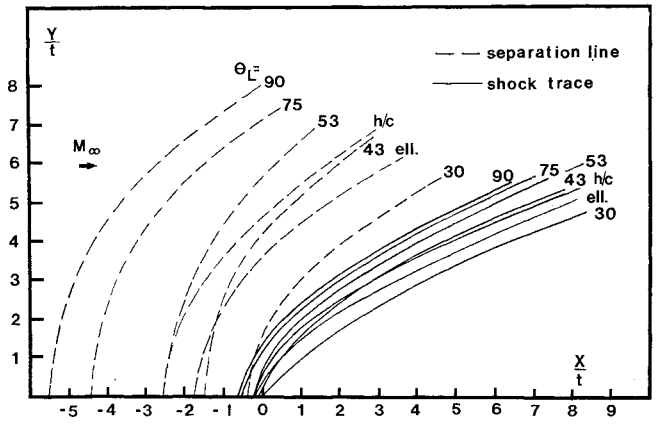

Fig. 11 Separation line and inviscid shock wave traces.

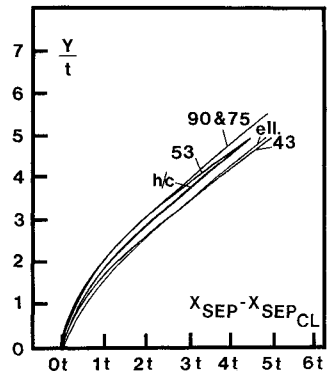

Fig. 12 Spanwise growth rate of separated flow upstream of shock wave.

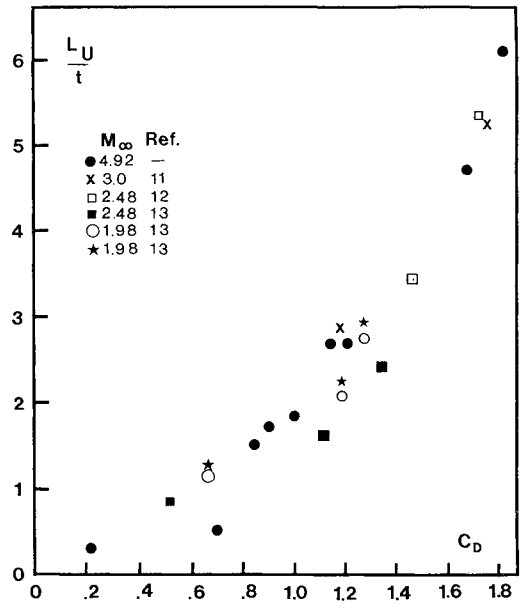

Fig. 13 Centerline separated flow length as a function of C_D.

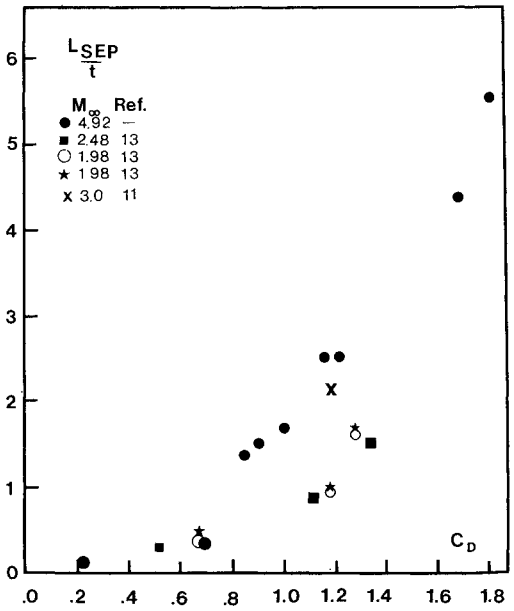

Fig. 14 Centerline upstream influence as a function of C_D.

where K depends on the wedge half-angle and is given by $K=\sin^{1/5}(\theta_L/2)$. $C_p'=(P_{02}-P_\infty)/q_\infty$ where P_{02} is the stagnation pressure downstream of a normal shock, P_∞ the upstream static pressure, and q_∞ the upstream dynamic pressure. The results for all leading edges tested and for the data of Refs. 11 and 12 are shown in Figs. 13 and 14, respectively.

Implicit in the correlation parameters of the two figures is the idea of a first-order dependence of L_u and L_{sep} on inviscid parameters. Even though there is significant scatter, this basic idea is partly supported by Fig. 13 but not by Fig. 14 in which systematic effects of Mach number changes are evident. It is unlikely that the discrepancies could be attributed to errors in estimating L_{sep}; different observers can consistently bracket it with $\pm 0.2t$. Similarly, errors in C_D are also an unlikely cause; an error of $\pm 10\%$ would not alter the qualitative observation.

Close inspection of the different tests forming the data set, notably the Mach 5 results that spanned the wider range of model geometries, suggests that at a fixed M_∞ a reasonable correlation with C_D is obtained for both quantities. The data points for the elliptic and hemicylindrical leading edges with $C_D=1.0$ and 1.21, respectively, correlate well with the wedge leading edges. The data points for hemicylindrical and 90 deg wedge fins at Mach 3 also correlate well with the Mach 5 data. Although the tests were not performed, Reynolds number changes would probably not affect the correlation significantly, particularly that for L_{sep}. As noted earlier, detailed experimental data for the hemicylindrical case over a broad range of Reynolds numbers have shown only a very weak dependence. As the flow structure is similar for all cases for $\theta_L > 43$ deg (i.e., $C_D > 0.84$), it is likely the same independence of Reynolds number exists for each of the other geometries. This independence is supported by the Mach 1.98 data in both figures.

The correlation with drag coefficient, even for the more limiting case of fixed Mach number is interesting from a fundamental standpoint as well as being useful from an engineering point of view. Approximate flow-length scales for an arbitrary shaped leading edge can be estimated quickly and easily. This can be particularly useful in the early phase of wind-tunnel experiments when decisions must be taken on model sizes and the locations of test surface instrumentation. From the fundamental point of view, the fact that at fixed Mach number the length scale of the separated flow can be correlated reasonably well in terms of an inviscid parameter, lends further support to the idea that inviscid mechanisms play a very important role. This latter idea has arisen from the observed independence of the interaction length scales on boundary-layer (i.e., viscous) parameters in hemicylindrically blunted fin flows and is supported both by experiment and computations.[3,5,9,10] The current results suggest that this inviscid dominance applies to a broader class of fin-induced flows than that specific geometry.

The implications of this result for numerical simulations is not at all clear. To date, as far as the authors are aware, only one computation of this class of flow has been made.[9,10] A finite-volume algorithm implementing MacCormack's explicit-implicit predictor-corrector method was used to solve the Navier-Stokes equations. The Baldwin-Lomax model with a modified length scale was used for turbulence closure. Comparisons of the solution with the measurements of Ref. 5 for a hemicylindrically blunted fin flow were quite impressive. The main features of the flowfield, such as the peak pressures on the fin leading edge, and the double-peaked centerline pressure distributions were closely predicted. Moreover, the experimentally observed independence of the flow length scales on the incoming boundary-layer thickness was also predicted. The present work raises some intriguing questions about such flow simulations. First, if the underlying mechanisms are largely inviscid, simplified forms of the Navier-Stokes equations may capture the general features and approximate length scales. Full Navier-Stokes codes may only be required for capturing the finer details of the flow

structure. In the same vein, whether or not accurate turbulence modeling is necessary is also very much an open question and worthy of further investigation.

Conclusions

An experimental study has been made of the effects of leading-edge geometry on the upstream influence and separated flow-length scales in blunt fin-induced shock wave turbulent boundary-layer interaction at Mach 5. The fins tested were all semi-infinite and included elliptic, hemicylindrical, and wedge-shaped leading edges. The results show that:

1) For wedge-shaped leading edges with half-angles of about 30 deg and above, both the centerline upstream influence and separated flow length scales increase linearly with wedge angle. The scales are large and upstream influence varies from 0.5 fin thicknesses at 30 deg to 6 fin thicknesses at 90 deg. Over the same range of angles, the separated flow length scale increases from 0.4 to 5.5 fin thicknesses.

2) For wedge half-angles close to shock detachment and above, the centerline pressure distributions have the classic shape associated with hemicylindrically blunted fin flows. For half-angles of 75 and 90 deg, secondary separation develops. At these high angles, the pressure distributions are effectively geometrically similar.

3) The qualitative features of the pressure distributions and the linear variation of the flow length scales with wedge angle are in good agreement with the recent data of Saida et al. at Mach numbers of 1.98 and 2.48.

4) Fin leading-edge shape has a large effect on the centerline separated flow length scale but does not affect its spanwise growth rate.

5) The Mach 5 centerline upstream influence and separated-flow length scales generated by different leading edges can be correlated with fin leading-edge drag coefficient. Attempts to correlate additional data at Mach 1.98 and 2.48 from other studies resulted in a reasonable correlation for upstream influence, but that for the separation length showed a clear Mach number influence.

6) The observation that upstream influence can be correlated in this form over a range of Mach numbers, and that the separated flow length can be correlated at a fixed Mach number, supports the view that in these fin-induced interactions, inviscid mechanisms play an important role.

Acknowledgments

The assistance of Eddie Zihlman, wind tunnel technician, Richard Gramann, graduate student, and the Bureau of Engineering Research of the College of Engineering is gratefully acknowledged, as are the suggestions made by Professor John Stollery, College of Aeronautics, Cranfield Institute of Technology, Cranfield, UK.

References

[1]Price, A. E. and Stallings, R. L., "Investigation of Turbulent Separated Flows in the Vicinity of Fin Type Protuberances at Supersonic Mach Numbers," NASA TN D-3804, Feb. 1967.

[2]Westkaemper, J. C., "Turbulent Boundary Layer Separation Ahead of Cylinders," *AIAA Journal,* Vol. 6, July 1968, pp. 1352–1355.

[3]Sedney, R. and Kitchens, C. W. Jr., "Separation Ahead of Protuberances in Supersonic Turbulent Boundary Layers," *AIAA Journal,* Vol. 15, April 1977, pp. 546–552.

[4]Dolling, D. S. and Bogdonoff, S. M., "Scaling of Interactions of Cylinders with Supersonic Turbulent Boundary Layers," *AIAA Journal,* Vol. 19, May 1981, pp. 655–657.

[5]Dolling, D. S. and Bogdonoff, S. M., "Blunt Fin-Induced Turbulent Boundary Layer Interaction," *AIAA Journal,* Vol. 20, Dec. 1982, pp. 1674–1680.

[6]Dolling, D. S., "Comparison of Sharp and Blunt Fin-Induced Shock Wave/Turbulent Boundary Layer Interaction," *AIAA Journal,* Vol. 20, Oct. 1982, pp. 1385–1391.

[7]Hung, F. T. and Clauss, J. M., "Three-Dimensional Protuberance Interference Heating in High Speed Flow," AIAA Paper 80-0289, Jan. 1980.

[8]Ozcan, O. and Holt, M., "Supersonic Separated Flow Past a Cylindrical Obstacle on a Flat Plate," *AIAA Journal,* Vol. 22, May 1984, pp. 611–617.

[9]Hung, C. M. and Kordulla, W., "A Time Split Finite Volume Algorithm for Three Dimensional Flow-Field Simulation," AIAA Paper 83-1957, July 1983.

[10]Hung, C. M. and Buning, P. G., "Simulation of Blunt Fin-Induced Shock Wave and Turbulent Boundary Layer Interaction," AIAA Paper 84-0457, Jan. 1984.

[11]Dolling, D. S. and Bogdonoff, S. M., "Experimental Investigation of Three Dimensional Shock Wave Turbulent Boundary Layer Interaction: An Exploratory Study of Blunt Fin-Induced Flows," Gas Dynamics Laboratory, Princeton University, Princeton, NJ, MAE Rept. 1468, March 1980.

[12]Saida, N., "Separation Ahead of Blunt Fins in Supersonic Turbulent Boundary Layers," *Proceedings of the IUTAM Symposium on Turbulent Shear Layer/Shock Wave Interaction,* (1985), Springer-Verlag, 1986, pp. 247–258.

[13]Rodi, P. E., "An Experimental Study of the Effects of Leading Edge Geometry in Blunt Fin-Induced Shock Wave/Turbulent Boundary Layer Interactions," M.S. Thesis, Department of Aerospace Engineering and Engineering Mechanics, University of Texas at Austin, TX, May 1986.

[14]Settles, G. S. and Teng, H. Y., "Flow Visualization Methods for Separated Three Dimensional Shock Wave/Turbulent Boundary Layer Interaction," *AIAA Journal,* Vol. 21, March 1983, pp. 390–397.

[15]Winkelmann, A. E., "Experimental Investigations of a Fin Protuberance Partially Immersed in a Turbulent Boundary Layer at Mach 5," Naval Ordnance Lab., TR-72-33, Jan. 1972.

[16]Hung, C. M., private communication 1985.

[17]Gramann, R. and Dolling, D. S., "Unsteady Separation in Shock Wave Turbulent Boundary Layer Interaction," AIAA Paper 86-1033, May 1986.

[18]Dolling, D. S. and Narlo, J. C. II, "Driving Mechanisms of Unsteady Separation Shock Motion in Hypersonic Interaction Flow" *Proceedings of the Agard Conference on Aerodynamics of Hypersonic Lifting Vehicles,* Agard 428, Nov. 1987.

[19]Andreapoulos, J. and Muck, K. C., "Some New Aspects of the Shock Wave Boundary Layer Interaction in Compression Ramp Flows," AIAA Paper 86-0342, 1986.

[20]Hoerner, S. F., *Aerodynamic Drag,* (published by the author), Great Britain, 1965.